Final Draft
of the original manuscript:

Mechanical and failure behaviour of hybrid polymer–metal staked joints

A.B. Abibe [a,b] – andre.abibe@hzg.de
S.T. Amancio-Filho [a,b,*] - sergio.amancio@hzg.de
J.F. dos Santos [a] – jorge.dos.santos@hzg.de
E. Hage Jr [c] – elias@ufscar.br

[a] Helmholtz-Zentrum Geesthacht, Institute of Materials, Materials Mechanics, Solid State Joining Processes (WMP) – Max Planck Strasse 1, D-21502 Geesthacht, Germany
[b] Helmholtz-Zentrum Geesthacht, Institute of Materials Research, Materials Mechanics, Advanced Polymer-Metal Hybrid Structures Group – Max Planck Strasse 1, D-21502 Geesthacht, Germany
[c] Federal University of São Carlos (UFSCar), Department of Materials Engineering (DEMa) – Rod. Washington Luiz km 235, CEP 13565-905, São Carlos-SP, Brazil.

*Corresponding author:
Sergio de Traglia Amancio-Filho
Max-Planck Strasse 1, D-21502 Geesthacht, Germany
Tel: +49 4152 87 2066
Fax: +49 4152 87 2033
sergio.amancio@hzg.de

Abstract

Structural applications that use multi-material structures in the transportation industry have increased in recent years. Weight reduction in order to avoid excessive emissions is the driving force of this trend. The current joining technologies for such complex structures have potential for engineering and performance improvement. This preliminary study shows an alternative joining method for hybrid structures, the so-called Injection Clinching Joining (ICJ) [Abibe et al., J Thermoplast Compos 2011, 24:2; 233-49], based on the principles of staking, injection moulding, and mechanical fastening. The main objectives of the paper are to exploit the mechanical behaviour of overlap joints produced by this proposed method and assess its potential as an applicable technology. The measurements used in this research are optical and scanning electron microscopy, X-ray computer microtomography, lap-shear strength testing and *in situ* strain distribution. Different failure modes were found, depending on the joining conditions. Net tension failure had a brittle and catastrophic nature, while rivet pull-out presented a more desirable slow ductile failure mode. The joint strengths were good, ranging from 35,9% to 88,5% of the base material's experimental ultimate tensile stress. Although there is a lack of studies on structural staking applications, this paper shows potential for these joining techniques and introduces ICJ as a potential focus of future research.

Keywords: hybrid structure, short fibre composite, staking, polymer-metal joining, failure mode, moisture content

1. Introduction

The selection of structural materials in transportation vehicles is undergoing a transition phase. Previously produced out of steel, automotive body-in-white parts are increasingly using fibre reinforced plastics (FRP) and lightweight metals such as magnesium and aluminium alloys. Similar changes are occurring in the aircraft industry, which currently aims for a 50% composition of FRP in structural parts. The driving force for such efforts in manufacturing technology is the increased energy efficiency of the vehicles, mainly due to world fuel economy demands and the desire to reduce emissions [1].

The presence of assorted materials renders the joining process of the structure complex. Current joining technologies of adhesive bonding and mechanical fastening are often unable to fulfil the industry requirements. Moreover, the design of multi-material joints in transportation must consider the possibility of catastrophic failure and the avoidance of such failures.

In hybrid systems with a large dissimilarity in mechanical properties between the joining partners, failure is most likely to happen at the weakest component. Figure 1 shows the expected failure types on bolted joints, according to ASTM D5961 (ASTM: D5961). Net tension, cleavage, shear-out, and tear-out are the catastrophic failure modes, whereas bearing failure is caused by the buckling of the material and only gradually causes the loss of load sustainability [2]. Slow failure mechanisms such as bearing are preferred in mechanical fastening over the unpredictability of a catastrophic failure. In consideration of this preference, the geometric relations of the structure can be designed by engineers to induce a most probable failure mode. For example, Içten et al. [3] studied the effect of joint geometry on joint behaviour and learned that large "width-to-diameter" and "edge distance-to-diameter" ratios will lead to bearing failure, while small values of these ratios are likely to induce net tension or shear-out failure. Similar evaluations of geometric parameters on laminate composite joints were studied by Sen et al. [4] and Wang et al. [5], and by Yilmaz and Sinmazçelik [6] on a short fibre reinforced composite. All groups observed the strong influence of correct design of joining components for good mechanical performance and predictable failure modes. Materials selection and tailoring of properties are also important considerations to obtain soundly assembled structures.

In recent years, several experts have studied ways of assembling multi-material structures, and they have assessed failure modes and the mechanical behaviour of hybrid joints. Içten et al. [3] evaluated failure prediction on mechanically fastened Kevlar-epoxy composites by using numerical models and experimentation to validate failure modes and load carrying capacities with respect to joint geometry. Hundley et al. [2] contributed to the topic with a work regarding bolted polymer-metal laminates and their failure mechanisms through computation and experimentation. Jung et al. [7] produced bolted-joint and beam-joint multi-material structures for railway vehicles. Static and dynamic testing was performed to analyse failure modes and fatigue life. In the field of hybrid joining techniques, Kweon et al. [8] have identified correlations between the properties of metal composite joints and the joining mechanisms used. Their comparison of bonded, bolted, and hybrid bolted-bonded joints of the same materials showed that hybrid joining is only a benefit when a bolted joint of the same type is more efficient than the bonded joint; otherwise, the hybrid is prejudicial to the bonding mechanism of the adhesive. This effect was also shown for dissimilar

aluminium-steel joints by Moroni et al. [9]. Bolted joint properties are also improved by the use of z-direction reinforcements in polymer matrix composites, which are most commonly represented by z-pins. Their use on laminate composites increases delamination toughness, impact damage tolerance, static joint strength, and joint fatigue life [10]. In a study of bolted joints with z-pin reinforcement around the bolt, Li et al. [11] concluded that this feature significantly increases the bearing properties of the joints. Many papers focus on the current concepts of integral structures with great damage tolerance and fatigue resistance, both of which are of great importance to the transportation industry.

Abibe et al. [12] recently introduced the "Injection Clinching Joining" (ICJ) process as an alternative technique to join multi-material structures. This process is based on staking, injection moulding, and mechanical fastening, and it was shown to have the potential to be optimised for future industrial applications. The current contribution evaluates the failure behaviour of ICJ joints, as well as the relationship between material properties and joint failure. The observations shown here are important to the understanding and improvement of staking-based technologies for multi-material structures.

2. Materials and methodology

The materials were chosen by considering the target applications of the structures in transportation. The polymeric partner was a polyamide 6,6 reinforced with 30% short glass fibres (Ertalon 66-GF30, Quadrant Plastics, Lenzburg, Switzerland), which is common in automotive under-the-hood components; the metallic partner was an aluminium alloy, 2024-T351 (Rio Tinto Alcan, Montreal, Quebec, Canada), used in engineering structures.

Short glass fibre-reinforced polyamide 6,6 (PA66-GF) and aluminium 2024-T351 joints were produced using the Injection Clinching Joining process [12, 13]. This is a staking joining technology for multi-material structures which can join polymers or polymer composites to other materials – metals, ceramics or other polymer-based compounds. For a more detailed description of the process and highlights of its development, please refer to Abibe et al. [12].

A description of the process is shown in Figure 2. A polymer-based part with a protruding stud is pre-assembled with a joining partner that contains a through hole so that the stud fits in the hole. The hot case and punch-piston tool system approaches the pre-assembled parts, with the hot case containing the polymeric stud (Figure 2a). The stud is heated at a certain processing temperature for a predetermined joining time (Figure 2b), after which the punch-piston pushes the molten/softened polymer into the hole (Figure 2c). Then, the system is cooled under pressure to reduce the polymer thermal relaxation, and the joint is consolidated (Figure 2d). By the end of the process, a joint is obtained in which there are no additional parts other than the joining partners, with the polymeric stud working as a rivet to the joint.

ICJ joints make use of cavity profiles in the through-holes of the joining partner. The molten/softened polymer fills the cavity, remains anchored after the joint cools and then consolidates; the mechanical performance is improved by the additional anchoring performance provided by the cavity profile. Examples of possible cavities are chamfers and profiles such as threaded or dove-tailed.

This investigation used different combinations of heat input to the polymer composite by varying the joining time and processing temperature. Joints were produced using as-received PA66-GF and two different drying conditions to account for the influence of water content on mechanical behaviour. The PA66-GF parts were dried in a convection oven prior to joining. A summary of the joining parameters is presented in Table 1.

The process parameters were changed for each condition following a ''one factor at a time'' (OFAT) approach, based on the parameters of the reference condition, ''Ref''. In this way, the isolated effects of the parameters can be interpreted in terms of specific response changes. Analysis of variance (ANOVA) was used to evaluate the significance of these effects. The ANOVA calculated the F factor using the F-test for the rejection of the null hypothesis for the factors with no significant influence on the response. Calculations were performed with OriginPro 8 from OriginLab for a significance level (α) of 5% (confidence level of 95%). Assessment of the mechanical behaviour of the ICJ joints was performed with lap shear strength (LSS) testing of single lap joints (Figure 3). The mechanical performance could be determined and

the strain distribution graphically monitored during the testing process. Fracture surface analysis and X-ray microtomography imaging were performed on the tested samples.

Lap shear strength testing was performed using a Zwick 1478 universal testing machine (Zwick/Roell, Ulm, Baden-Württemberg, Germany) with a 2 mm/min traverse speed at room temperature in a procedure based on the standard D5961 (ASTM: D5961). Three replicates for each processing condition were tested, and their maximum loads were recorded. Standard D5961 evaluates the bearing stress of bolted joints; in this case, the bearing stress was determined between the surfaces of the metallic plate and the polymeric rivet. The bearing stress can be calculated with Equation 1:

$$\sigma_i^{br} = \frac{P_i}{k \times D \times h} \qquad (1)$$

In equation 1, σ_i^{br} is the bearing stress in MPa, P_i is the load borne by the joint in N, k is a geometrical factor (of value equal to 1 for single hole joints), D is the diameter of the hole in mm, and h is the thickness of the plate in mm.

The PA66-GF specimens were dried prior to the joining process. The as-received material was heated for 24 hours at 60 °C and at 120 °C. Three resulting groups of material conditions were evaluated: as-received, dried at 60 °C, and dried at 120 °C. Lap shear strength testing of the ICJ joints was performed for these specimens.

Scanning electron microscopy (SEM) was used to observe the fracture surfaces. Magnifications of up to 2000 times enabled identification of material failure features. X-ray computer microtomography was used to observe the internal features of the joints after failure. The strain distribution of the overlap samples was monitored *in situ* during lap shear testing using the ARAMIS® system (GOM mbH, Braunschweig, Niedersachsen, Germany). This system uses digital image correlation and tracking technology on the surface of the material, being able to calculate deformation of the studied surface. In this technique, the samples are sprayed with a layer of white paint and another layer of sparse black paint, forming a dotted pattern on a white background. The system reads the relative movement between the dots and calculates strain distributions on the material surface during the test. This method was used to graphically show the details of the different failure types during lap shear testing.

3. Results and discussion

3.1. Behaviour of ICJ-staked Joints under Static Loading

ICJ overlap joints were tested for lap shear strength in the universal testing machine. Figure 4 shows the behaviour of the joints during this test, in which it is possible to identify the typical stages of load bearing in the ICJ-staked joints. The sequence of pictures from (a) to (e) corresponds to the points on the load-displacement plot. The linear part of the curve (point a) relates to the elastic regime. After this point, the rivet tends to rotate out of the plane parallel to the loading direction – secondary bending –, as shown by the arrow on Figure 4b. The rivet rotation leads to reduction of the load, which corresponds to a loss of excess material on the superior surface of the metallic plate (point c). At this point, the load is sustained by the rivet itself, supported by the internal wall in the cavities of the metallic partner. As the deformation continues, the plates slowly separate from each other, reducing the bearing load (point d) until complete loss of mechanical resistance is achieved (point e). At this stage, the rivet is torn from its base, causing a crack to nucleate and propagate through the plaque thickness. The turning point in this case is the rotation stage of the rivet, which initiates the process of secondary bending of the composite plaque. The process can be hindered by a larger contact volume on the superior surface of the metallic plate or by improving cavity filling in the joint.

The fracture regime can be better analysed through X-ray computer microtomography. An ICJ joint tested for lap shear strength was observed with this technique. Figure 5a shows the *post-mortem* investigation containing an overview of the cross-section of a tested ICJ joint. Secondary bending of the composite plaque due to the rotation of the rivet is shown. The rivet is still being supported by the walls of the cavities in the metallic plate. Figure 5b displays the material volume that was originally in contact with the surface of the chamfer, hindering rivet rotation. A stress concentration is created by the combination of pulling from the plaque and the support of the rivet by the walls of the hole in the region between the plaque and the rivet (Figure 5c). A crack nucleates (region 1), culminating in the rivet being pulled out (region 2).

This predominant failure behaviour in staked joints produced by ICJ develops due to the rotation of the rivet. A main crack nucleates at the base of the rivet, propagating towards the inferior surface of the composite plaque (see Figure 6a). Additionally, secondary bending induces a radial crack on the top of the rivet on the opposite side of the loading direction, detaching the volume of material on the chamfer from the rest of the rivet (Figure 6b). The continued rotation of the rivet (Figure 4b) causes these two cracking modes to take place simultaneously. Figure 6c presents a cross-section of a sample tested for lap shear strength with the nucleation sites described.

Rivet geometry features, such as large volumes of material on top of the chamfer and efficient cavity filling, hinder rotation of the rivet during lap shear testing. Figure 7 displays cross-sections of three overlap-tested joints and their failure modes and mechanical strengths. In Figure 7a, the material over the chamfer separated from the rest of the rivet. Regions 1 and 2 from Figure 7a display the small contact surface that fractured due to insufficient material volume over the chamfer. Moreover, this joint did not achieve filling of the screw cavities, resulting in a low mechanical resistance (1045 N).

A joint with a large amount of material on top of the rivet and partial filling of the cavities is shown in Figure 7b. The fracture occurred by tearing of the top portion of the rivet, splitting the rivet through its diameter along a preferential region, perpendicular to the length of the rivet. This direction of crack propagation can be an indicator of an interface with dramatic property changes, such as the transition from a thermomechanically affected zone to a thermally affected zone (e.g. a welding line). Further information about microstructural zones in ICJ joints can be found in [12]. Even when the filling of the cavities was not complete, it achieved nearly double the lap shear load (1937 N) of the joint in Figure 7a. This improvement helps to emphasise the contribution of the material volume over the chamfer to the improvement of the mechanical resistance.

In Figure 7c, a joint with a smaller volume on top of the chamfer but with an excellent filling of the screw cavity is shown. This joint displayed a slightly better mechanical performance (2059 N) than the specimen shown in Figure 7b. These characteristics indicate the beneficial effect of a filled cavity profile to the joint's mechanical performance.

The analysis of the geometrical changes obtained through the ICJ process and the correlation with the lap shear strength results lead to a few conclusions about the joint mechanical behaviour. Good surface finishing and optimisation of the joining partners' geometry are essential to hinder crack nucleation. For instance, the use of fillets on the base of the stud would reduce stress concentration, hampering the start of a crack akin to the one shown on Figure 6a. The correct choice of process parameters also plays a primary role, influencing the amount of heat input to the polymeric stud and its final shape after forming.

The factors that affect the heat input are the processing temperature and joining time [12] for the ICJ process. The shape of the formed rivet is related to the design of the cavities and is also influenced by the ability of the material to flow into these cavities. Therefore, the amount of structural water in the polyamide matrix and the deformation rate imposed on the material during processing may influence the viscosity of the composite, affecting the final geometry of the joint. The influence of the deformation rate was not investigated in this study, but the effects of heat input are shown in Figure 8. The joint in Figure 8a was processed at 250 °C for 1 minute and 30 seconds and shows a large volume of material on top of the rivet, at the expense of material in the screw cavities. This result indicates that the heat input was insufficient, so that the stud material could form a rivet head but did not flow into the cavities. In Figure 8b, the selection of a higher process temperature of 300 °C significantly reduced the molten viscosity, and the material flowed outside of the hot case, as indicated by the arrows. This outcome is also undesirable because the material is lost to the surroundings, instead of filling the cavities and leading to improved mechanical anchoring. The sample shown in Figure 8c is an example of excessive heat input to the materials. The temperature used, 350°C, is much higher than the crystalline melting point of polyamide 6,6, and long application of such high temperatures compromises the integrity of the composite. Although the cavities have good filling, the composite contains many volumetric defects, most likely due to the degradation of the polymer matrix and the evolution of structural water.

3.2. Effect of Polyamide Water Content on Mechanical Behaviour of ICJ Joints

Water content is an important technical issue in hydrophilic polymers. The attractive properties of polyamides in industrial applications can be impacted by their affinity with water, which may detrimentally impact their properties. The influence of water content on polyamides has been extensively investigated [14-17], as has its influence on joining and welding [18, 19]. The main factors impacted by absorbed water are the reduction of viscosity [16, 20], lowering of the glass transition temperature and hydrolysis during processing. Absorbed or structural water acts as a plasticiser in polyamides, promoting chain movement, which in turn impacts processing, dimensional stability and mechanical properties [21]. Its impact on the thermo-oxidative degradability of polyamide 6,6 is also important. The chain scission mechanism comes from thermoxidative attack on the α-carbon, which eventually generates an imide group or hydroxylated amide on the chain. These points are favourable for hydrolytic chain scission [14], which contributes to strength reduction.

As the literature describes [21], dry PA66 should present a more brittle yet stronger tensile performance than atmosphere-conditioned PA66. In this study, PA66-GF was joined in the as-received state, meaning that any water absorbed after its extrusion by the supplier, through transportation and storage, was retained. Two drying treatments of the PA66-GF composites were tested to account for the retained water effect on joint properties. The impact of water content on the mechanical behaviour of PA66-GF/AA2024-T351 ICJ joints is similar to the effects stated in the literature for the mechanical properties of polyamides. Table 1 shows the drying conditions prior to joining of the PA66-GF parts for 24 hours at 60 °C and 24 hours at 120 °C in a convection oven.

Joints produced with as-received PA66-GF ("AR-PA66" specimens) or PA66-GF dried at 60 °C for 24 hours ("60C-PA66" specimens) presented ductile fracture, while the specimens with PA66-GF dried at 120 °C ("120C-PA66" specimens) for 24 hours exhibited brittle fracture. The fracture surface of a 60C-PA66 joint is shown in Figure 9a. The polymer matrix yielded locally during the test, forming fibrils in the direction of pulling. In contrast, the fracture surface observed for 120C-PA66 joints (Figure 9b) is clearly of a brittle nature. The polyamide matrix has not yielded, and it is much smoother in comparison to Figure 9a. The spherical particles in Figure 9 were identified by electron dispersive X-ray spectroscopy as organic compounds, possibly an elastomeric toughening/filling material [22].

These different characteristics are connected to the plasticising properties of water on polyamides [16, 20]. AR-PA66 and 60C-PA66 joints have enough water in the polymer matrix to relieve stresses better than the over-dried 120C-PA66 joints. The lack of water in the polymer renders the 120C-PA66 joints brittle and breakable, which significantly impacts the failure mode of the ICJ joint.

In situ graphical monitoring of strain distribution (ARAMIS, GOM mbH, Germany) during lap shear testing was used to assess the difference in the material failure mode. Figure 10a shows the painted surface of a lap shear specimen, and how it is displayed in the Aramis software at the beginning of a test (t = 0). The two drying condition behaviours are shown in the following images in a timeline (t1 < t2 < t3). The picture sequences show the different behaviours and failure modes for different drying conditions.

The sequence for the AR-PA66 specimens is similar to the one for the 60C-PA66 specimens. In these cases, the strain distribution is localised underneath the base of the rivet. This failure mode is characterised by rivet pull-out. Secondary bending on the polymer plaque promotes rotation of the rivet (Figure 5a), inducing crack nucleation and growth at its base, as described in Figure 5c. This is a slow and ductile process. In contrast, 120C-PA66 specimens display a catastrophic and brittle failure mode. The final failure of 120C-PA66 took 89 s (elongation of 2,96 mm). In comparison, the final failure of the 60C-PA66 specimens took 146 s (elongation of 4,87 mm), but the image sequence only shows the last frame before the paint detached from the specimen surface (t=130 s, elongation of 4,33 mm). Furthermore, the distribution of strain for the 120C-PA66 specimens is along the width of the plaque, with largest concentration at the base of the rivet; the final crack takes place perpendicular to the pulling direction. This type of failure is called net tension [23], which is a concept created for bolted joints (ASTM: D5961), but it has been observed in other point-on-plate joining processes [24-26]. Figure 10b and Figure 10c show the failure region in detail. In Figure 10b, the bending of the plaque and rotation of the rivet are visible, as is the final failure with the rivet apart from the plaque. Figure 10c presents the net tension failure, with the plaque broken instead of bent.

Although two different failure modes were observed for ICJ joints, the load-displacement curves for rivet pull-out and net tension failures are similar. In Figure 11, both curves present a first load peak corresponding to point (b) on Figure 4, followed by a decrease and a load plateau stage. For rivet pull-out failure mode, the load is sustained for a longer period, which corresponds to bearing of the rivet. In the net tension failure plot, the displacement is less than half of that from rivet pull-out behaviour, and it corresponds to the elongation of the base plaque of the polymeric material.

The most important statement about Figure 11 is the difference in displacement between the failure modes of the ICJ-staked joints. Net tension failure happens much faster than rivet pull-out failure. In the latter, the load is sustained for a longer time until a final failure occurs, while in the former it happens much earlier due to the brittle nature of the dry polyamide.

3.3. Mechanical Performance of ICJ Joints

A summary of the mechanical performance of ICJ joints is presented in Figure 12. The impacts of joining time (Figure 12a), processing temperature (Figure 12b) and drying treatment (Figure 12c) on the maximum load are shown with a comparison to the reference sample. The reference sample "Ref" achieved an average maximum load of 942 ± 77 N. Reducing the joining time raised the average value to 1112 ± 102 N (Figure 12a), while reducing the processing temperature improved the performance to 1807 ± 114 N (Figure 12b). Drying of the composite material yielded a positive effect, with the condition of 24 hours at 60 °C achieving 1114 ± 79 N, and 24 hours at 120 °C achieving 1208 ± 77 N (Figure 12c). The column diagram in Figure 12d shows that the processing temperature appears to have the most prominent effect.

Analysis of variance (ANOVA) was used as a tool to evaluate the significance of the effects of each parameter on the joint lap shear strength, based on the OFAT design of experiment from Table 1. For ultimate elongation, none of the studied parameters was significant according to the F-test in ANOVA. Furthermore, the region covered by

the extensometer contains the composite (which deforms plastically) and the metal (whose deformation is much lower than the composite); this deformation of the region of interest is not representative of the real strain/elongation of the joint. The ANOVA results for maximum load are summarised in Table 2.

In this experiment, the F-test determines whether a parameter influences the lap shear strength of the joint. A value of Prob(F) below the established significance level of 0,05 (α = 5%) indicates that the parameter effect is significant to the lap shear strength [27]. All the process parameters tested were evaluated as significant by the F-test. From the values of Prob(F) observed in Table 2, we have that the most influential parameter (the smaller the Prob(F) value the larger is the significance) is "process temperature", followed by "drying treatment", and the least influential is the "joining time". From the discussions from Figure 7 on the observation of the joint cross-sections and their behaviours during mechanical test, it is possible to discuss the results of ANOVA.

A shorter joining time (Figure 12a) of the composite results in a lower heat input, which in turn makes it more difficult to soften and deform the composite stud. This effect leads to less material being transferred to the cavities; however, a larger volume of material is maintained on top of the rivet, improving mechanical performance. The micrographs in Figure 12a show the difference in this contact volume between both joints. The same principle applies to the process temperature (Figure 12b). The reduction from 300 °C to 250 °C creates a much larger volume of material on top of the rivet, which contributes to load bearing during lap shear strength testing. Although the rationale for influence of process temperature and of joining time is the same, the effect of temperature is much more pronounced on the lap shear strength response. This observation is in agreement with the statistical results presented in Table 2, where the process temperature presented the largest influence on the lap shear strength. The drying treatment (Figure 12c) of the polyamide 6,6 exhibited the best result with 24 hours at 120 °C, followed by 24 hours at 60 °C and the as-received material (Ref). The micrographs show similar geometric features, and in this case the difference in mechanical performance is a reflection of the higher tensile strength of the polyamide 6,6 when dried due to the lack of plasticising effect from the retained water in the polymer matrix.

As for calculated bearing stresses, the single best observed ICJ joint (obtained during the preliminary study and therefore out of the investigated design of experiment) reached 51,5 MPa (2059 N), and the single worst observed joint (at condition "Ref") reached 20,9 MPa (835 N). The bearing stresses were calculated with Equation 1, from standard D5961 (ASTM: D5961). The as-received composite base material presented an ultimate tensile stress of 58,2 ± 1,19 MPa, tested according to DIN 53455 [28]. The stress-displacement curves for the best/worst joints and the averaged curve for the base material are shown in Figure 13. Therefore the joint mechanical performance for the tested material combinations varied from 35,9% to 88,5% of the composite base material.

4. Conclusions

The mechanical behaviour of staking joints produced by ICJ was described in this paper. The geometric, microstructural and failure characteristics of the joints could be correlated to the experimental mechanical properties. Two factors were considered important for ICJ-staked joints under static loading: a large volume of the rivet head in contact with the superior surface of the top joining partner; and effective cavity filling. This staking-based technique presented two modes of failure: net tension and rivet pull-out. Both failure modes are related to the bearing of the formed rivet against the internal walls of the hole in the metallic partner. The failure mode is directly connected to the water content (and therefore, brittleness) of the polymeric partner, PA66-GF. Joints in which the composite was dried for 24 hours at 120 °C failed catastrophically by net tension. Joints in which the composite was in the as-received condition or dried for 24 hours at 60 °C failed slowly by rivet pull-out. Although the ultimate tensile stress for the joints with dried composite is higher, a catastrophic failure is undesired in engineering applications, and ductile failure is preferred. The calculated bearing stress of the joints ranged from 35,9% (20,9 MPa) to 88,5% (51,5 MPa) of the experimental ultimate tensile stress of the base material. Overall, the mechanical performance of ICJ joints produced in this preliminary study was satisfactory, with room existing for improvement. As proposed, this study may provide a base for further improvements to structural multi-material staking applications.

References

[1] Amancio ST, dos Santos JF. Joining of Polymers and Polymer-Metal Hybrid Structures: Recent Developments and Trends. Polym Eng Sci. 2009;49:1461-76.

[2] Hundley JM, Hahn HT, Yang JM, Facciano AB. Three-dimensional progressive failure analysis of bolted titanium-graphite fiber metal laminate joints. Journal of Composite Materials. 2010;45:751-69.

[3] İçten BM, Karakuzu R, Toygar ME. Failure analysis of woven kevlar fiber reinforced epoxy composites pinned joints. Composite Structures. 2006;73:443-50.

[4] Sen F, Pakdil M, Sayman O, Benli S. Experimental failure analysis of mechanically fastened joints with clearance in composite laminates under preload. Mater Design. 2008;29:1159-69.

[5] Wang ZQ, Zhou S, Zhang JF, Wu XD, Zhou LM. Progressive failure analysis of bolted single-lap composite joint based on extended finite element method. Mater Design. 2012;37:582-8.

[6] Yilmaz T, Sinmazcelik T. Geometric parameters and chemical corrosion effects on bearing strength of polyphenylenesulphide (PPS) composites. Mater Design. 2007;28:1695-8.

[7] Jung DW, Kim JS, Choi NS. An experimental investigation of the static and fatigue fracture behaviour of hybrid composite/metal joints for a tilting car body. Fatigue & Fracture of Engineering Materials & Structures. 2009;32:744-51.

[8] Kweon J-H, Jung J-W, Kim T-H, Choi J-H, Kim D-H. Failure of carbon composite-to-aluminum joints with combined mechanical fastening and adhesive bonding. Composite Structures. 2006;75:192-8.

[9] Moroni F, Pirondi A, Kleiner F. Experimental analysis and comparison of the strength of simple and hybrid structural joints. International Journal of Adhesion and Adhesives. 2010;30:367-79.

[10] Mouritz AP. Review of z-pinned composite laminates. Composites Part A: Applied Science and Manufacturing. 2007;38:2383-97.

[11] Li R, Huong N, Crosky A, Mouritz AP, Kelly D, Chang P. Improving bearing performance of composite bolted joints using z-pins. Composites Science and Technology. 2009;69:883-9.

[12] Abibe AB, Amancio-Filho ST, Dos Santos JF, Hage E. Development and Analysis of a New Joining Method for Polymer-Metal Hybrid Structures. J Thermoplast Compos Mater. 2011;24:233-49.

[13] Amancio ST, dos Santos JF, Beyer M. Method and device for connecting a plastic workpiece to a further workpiece. United States: GKSS-Forschungszentrum Geesthacht GmbH (Geesthacht, DE); 2010.

[14] Gonçalves ES, Poulsen L, Ogilby PR. Mechanism of the temperature-dependent degradation of polyamide 66 films exposed to water. Polymer Degradation and Stability. 2007;92:1977-85.

[15] Jia N, Fraenkel HA, Kagan VA. Effects of Moisture Conditioning Methods on Mechanical Properties of Injection Molded Nylon 6. Journal of Reinforced Plastics and Composites. 2004;23:729-37.

[16] Kohan ML. Moisture in Nylon - Selected Topics. Annual Technical Conference of the Society of Plastics Engineers. Atlanta, USA: Society of Plastics Engineers; 1998. p. 1676-81.

[17] Kulkarni S, Hart D. Effect of overdrying hygroscopic resins and a technological solution for its prevention. Annual Technical Conference of the Society of Plastics Engineers. Nashville, USA: Society of Plastics Engineers; 2003. p. 736-40.

[18] Liu SJ, Chang IT. Optimizing the weld strength of ultrasonically welded nylon composites. Journal of Composite Materials. 2002;36:611-24.

[19] Kagan VA, Kocheny SA, Macur JE. Moisture effects on mechanical performance of laser-welded polyamide. Journal of Reinforced Plastics and Composites. 2005;24:1213-23.

[20] Khanna YP, Han PK, Day ED. New developments in the melt rheology of nylons. I: Effect of moisture and molecular weight. Polymer Engineering & Science. 1996;36:1745-54.

[21] Brydson JA. Polyamides and Polyimides. In: Brydson JA, editor. Plastics Materials. 7th ed. Oxford: Butterworth-Heinemann; 1999. p. 478-530.

[22] Abibe AB. Desenvolvimento de união de multimateriais através de "Rebitagem por Injeção" (Injection Clinching Joining): Universidade Federal de São Carlos; 2011.

[23] York JL, Wilson DW, Pipes RB. Analysis of the Net Tension Failure Mode in Composite Bolted Joints. Journal of Reinforced Plastics and Composites. 1982;1:141-52.

[24] Amancio ST. Friction Riveting: development and analysis of a new joining technique for polymer-metal multi-material structures. Welding in the World. 2011;55:13-24.

[25] Balakrishnan KN, Kang HT, Mallick PK. Joining aluminum to nylon using frictional heat. SAE World Congress. Detroit, USA: SAE International; 2007.

[26] Oliveira PHF, Amancio ST, dos Santos JF, Hage E. Preliminary study on the feasibility of friction spot welding in PMMA. Mater Lett. 2010;64:2098-101.

[27] Schmidt SR, Launsby RG. Understanding Industrial Designed Experiments. Colorado Springs: Air Academy Press & Associates; 2005.

[28] DIN. DIN 53455. Prüfung von Kunststoffen, Zugversuch. Hamburg: Deutsches Institut für Normung e.V.; 1981.

FIGURE CAPTIONS

(a) bearing (b) net tension (c) cleavage (d) shear-out (e) tear-out
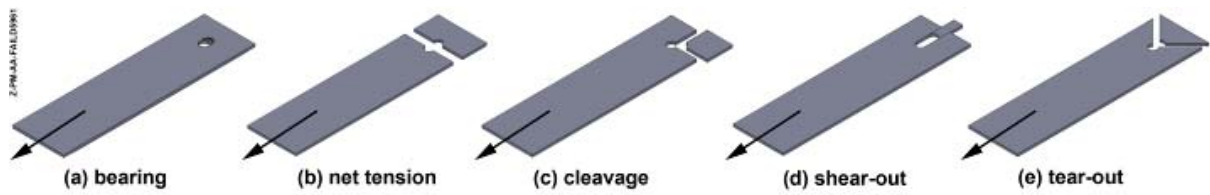
Figure 1: Failure types of bolted joints according to the standard D5961 (ASTM: D5961).

Punch-piston
Hot case
Joining partner
Polymer-based part

(a) Tool approaches the pre-assembled parts
(b) Hot case heats the stud on the polymer-based part
(c) Piston applies forming pressure on the stud
(d) Joined part

Joining Time
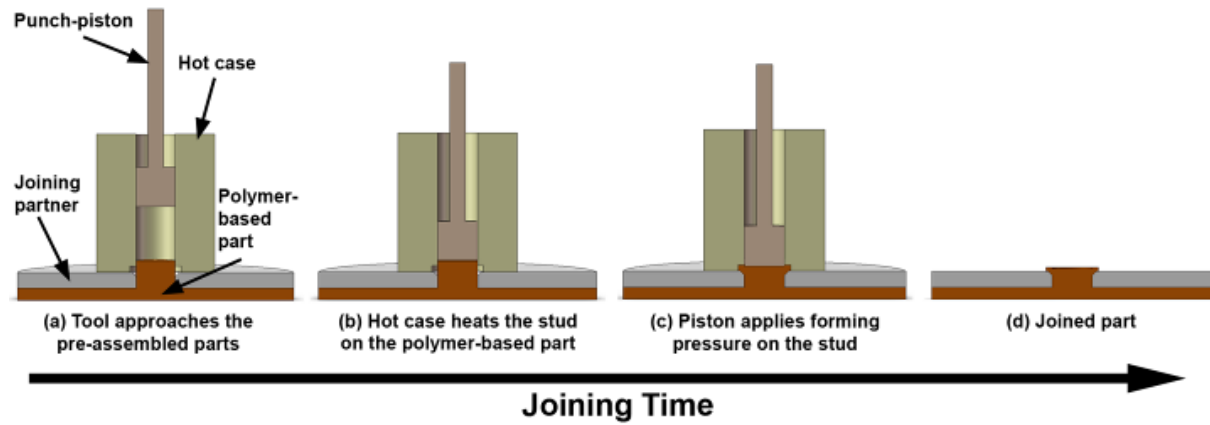
Figure 2: Steps of the ICJ process.

AA2024 10 mm diameter hole chamfer and screw

PA66-GF 9 mm diameter stud

123,5 mm
57 mm
28,5 mm
19 mm
38 mm
4 mm thickness
3 mm thickness
57 mm
123,5 mm
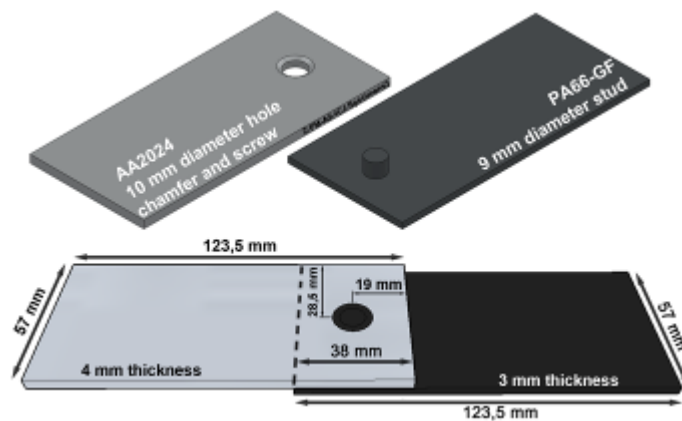
Figure 3: Geometry of overlap samples for the lap shear strength testing.

14
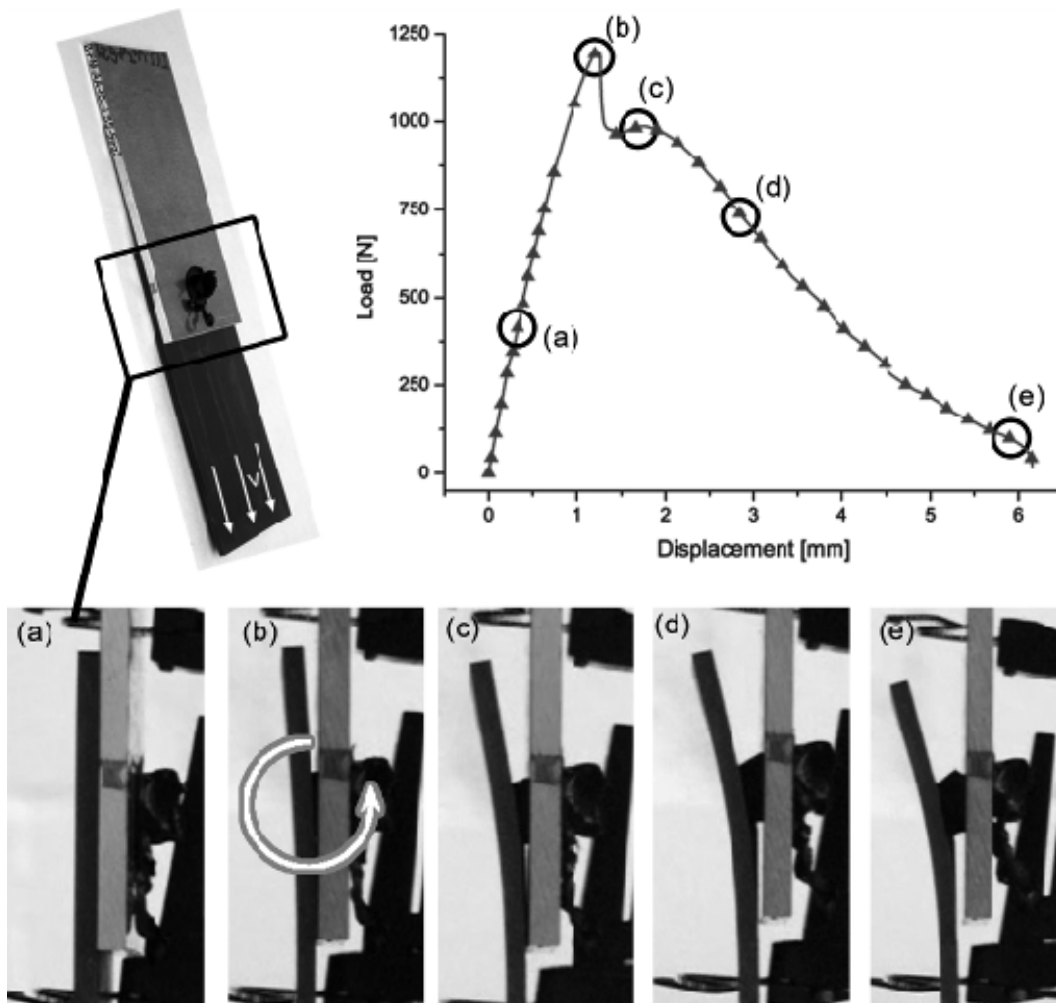
Figure 4: Typical behaviour of an ICJ joint when tested for lap shear strength: (a-e) stages observed during the test.
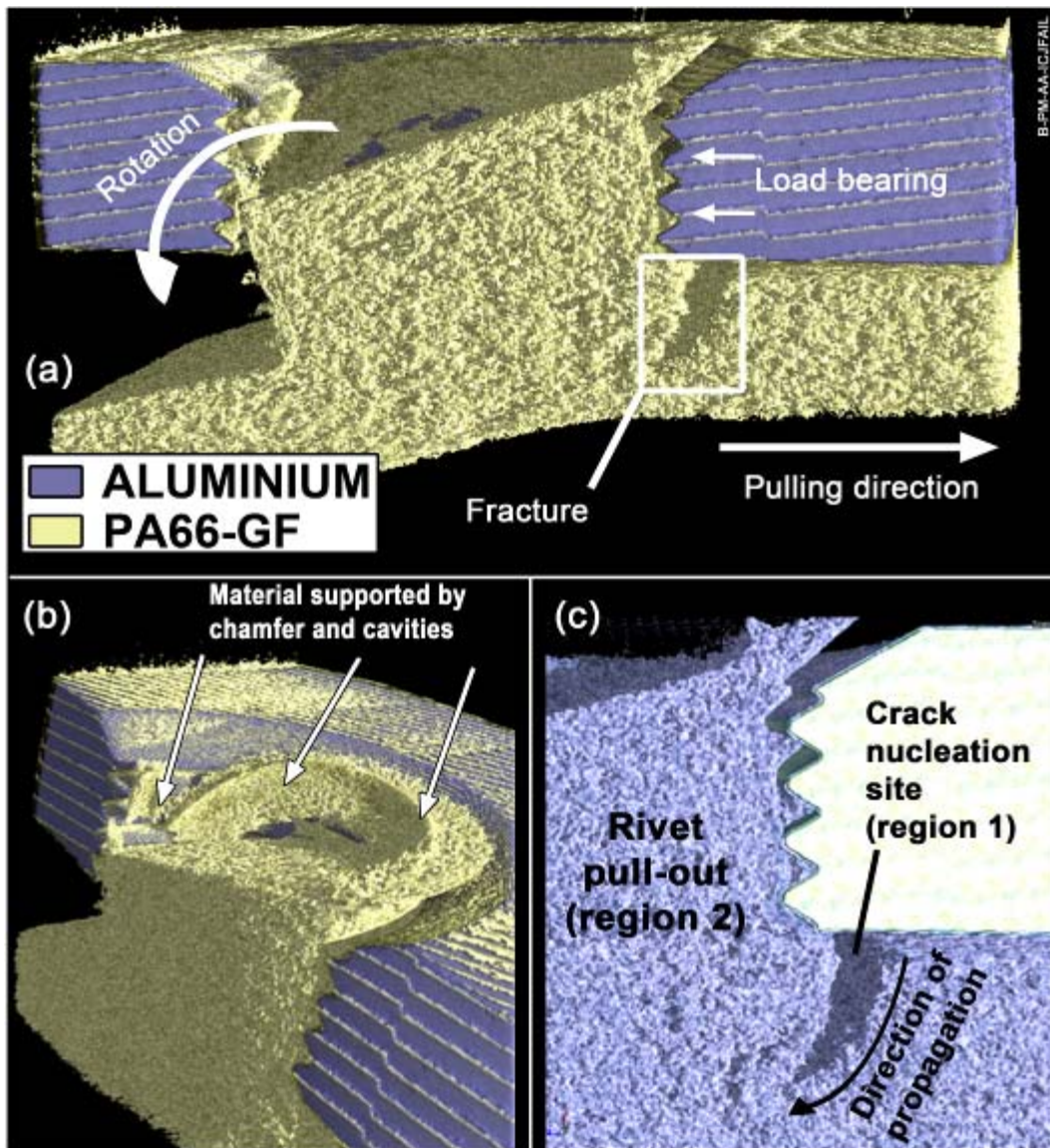
Figure 5: X-ray computer microtomography *post-mortem* analysis of the failure mechanism of an ICJ joint tested for lap shear strength: a) cross-section of the joint; b) top view, showing the material volume on top of the joint; c) detailed view of the crack nucleation site and path, as well as cavity filling.
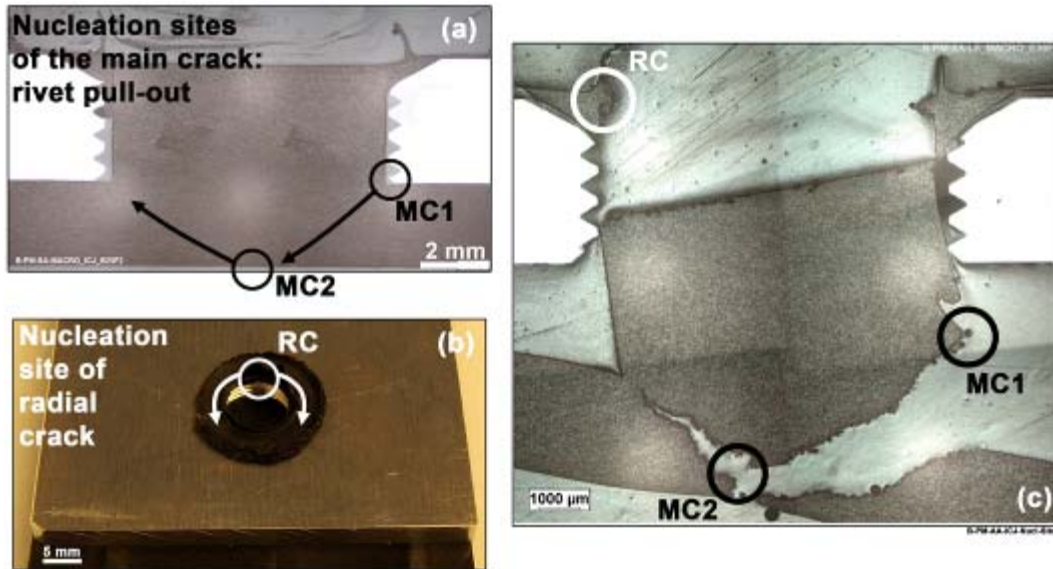
Figure 6: Crack nucleation sites on the ICJ overlap joints. a) main crack path on the base of the rivet, causing rivet pull-out; b) radial crack on top of the rivet; c) cross-section of a tested joint, highlighting the main crack (MC) and radial crack (RC) nucleation sites described on (a) and (b).
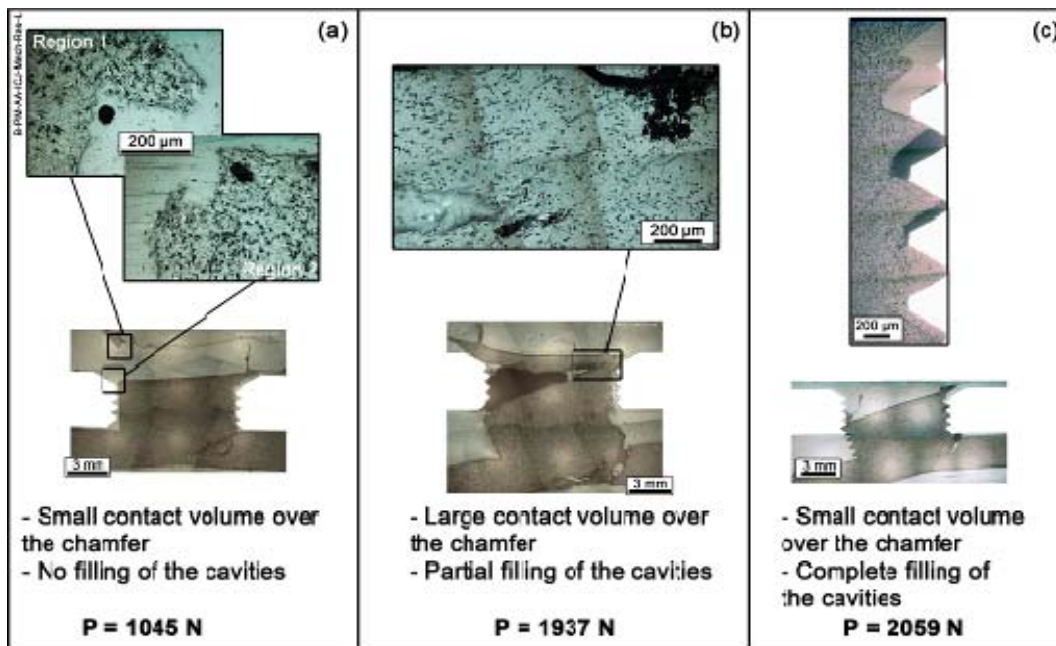
Figure 7: Rivet geometry effects on the mechanical resistance of ICJ joints. a) low resistance joint; b) good resistance joint, low cavity filling; c) good resistance joint, low volume on top of rivet.
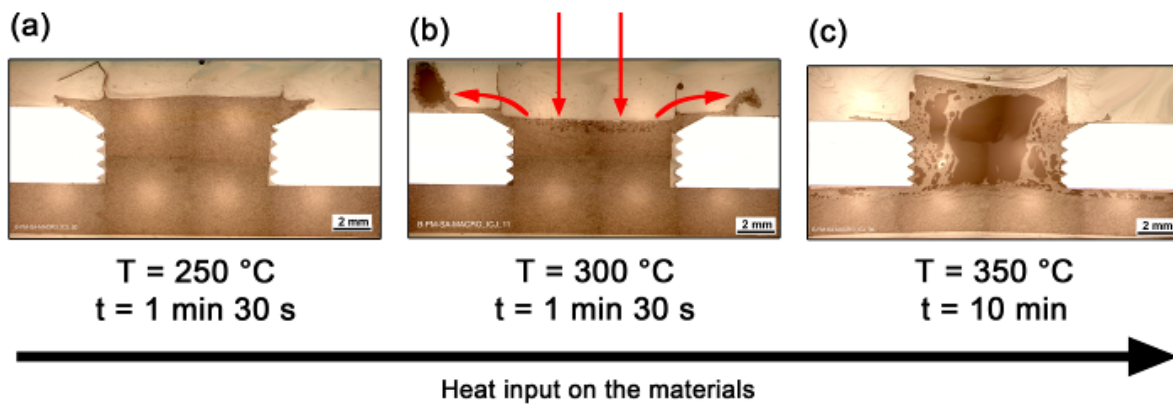
Figure 8: Effect of heat input on ICJ joint structure. a) low heat input; b) high heat input; c) excessive heat input.
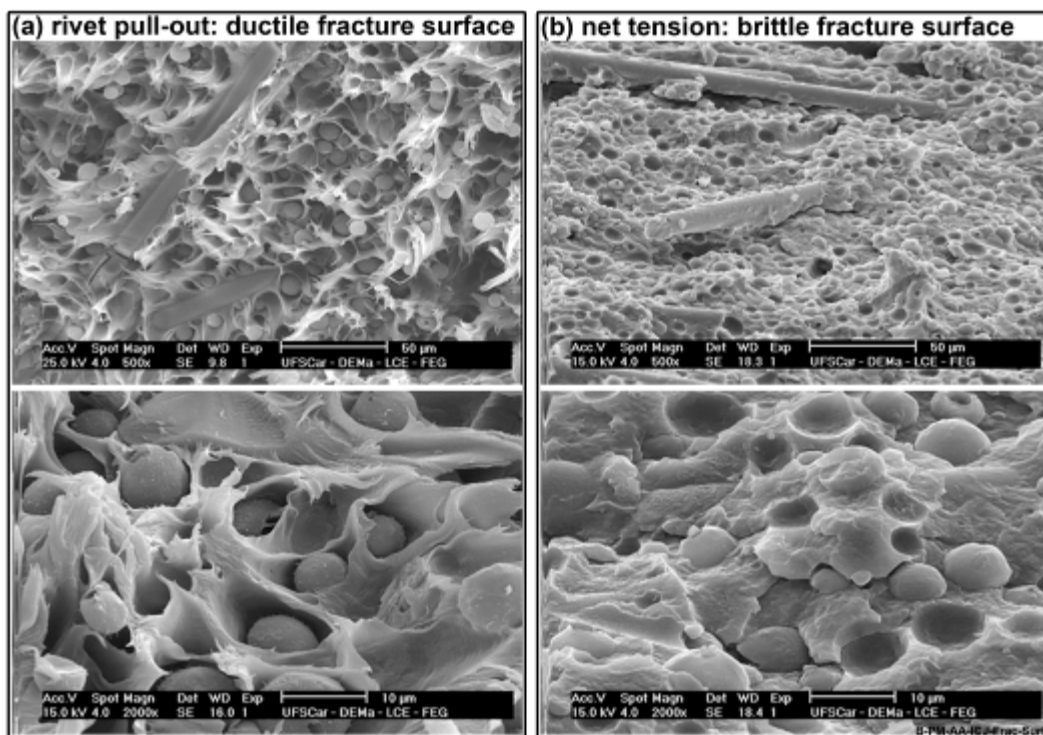

Figure 9: Fracture surface of PA66-GF composite of ICJ joint. a) rivet pull-out failure, ductile: condition "60C-PA66" (composite dried for 24 hours at 60 °C); b) net tension, brittle failure: condition "120C-PA66" (composite dried for 24 hours at 120 °C).
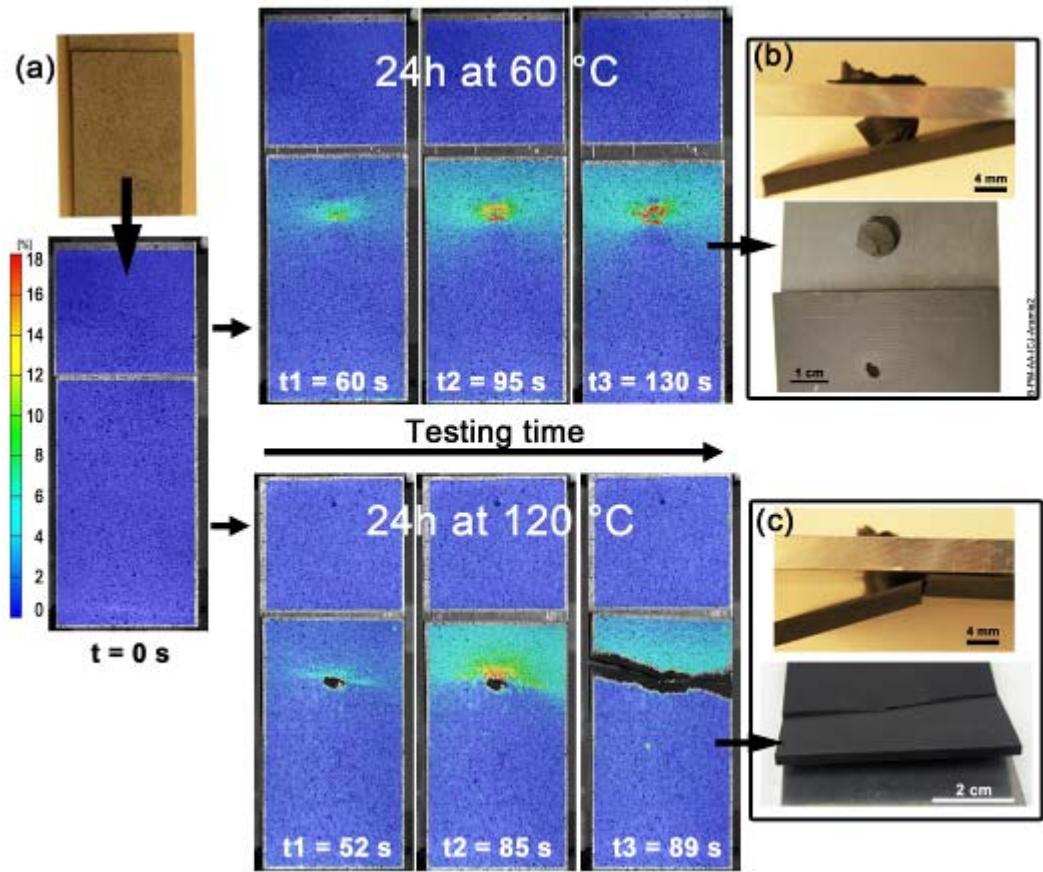
Figure 10: *In situ* strain distribution and failure behaviours of ICJ joints for different composite drying conditions. a) sample set up before testing and strain distribution over time for the composite dried under two conditions; b) rivet pull-out failure of condition "60C-PA66"; c) net tension failure of condition "120C-PA66".
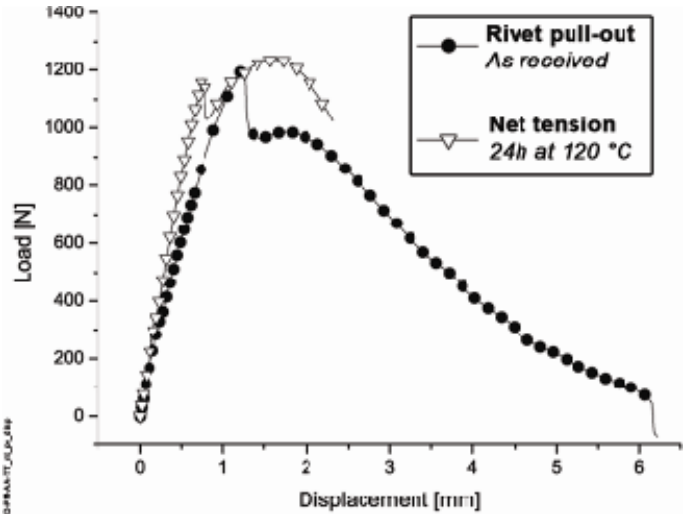

Figure 11: Load-displacement curves for rivet pull-out (condition "Time", with as-received composite) and net tension (condition "120C-PA66") failures.
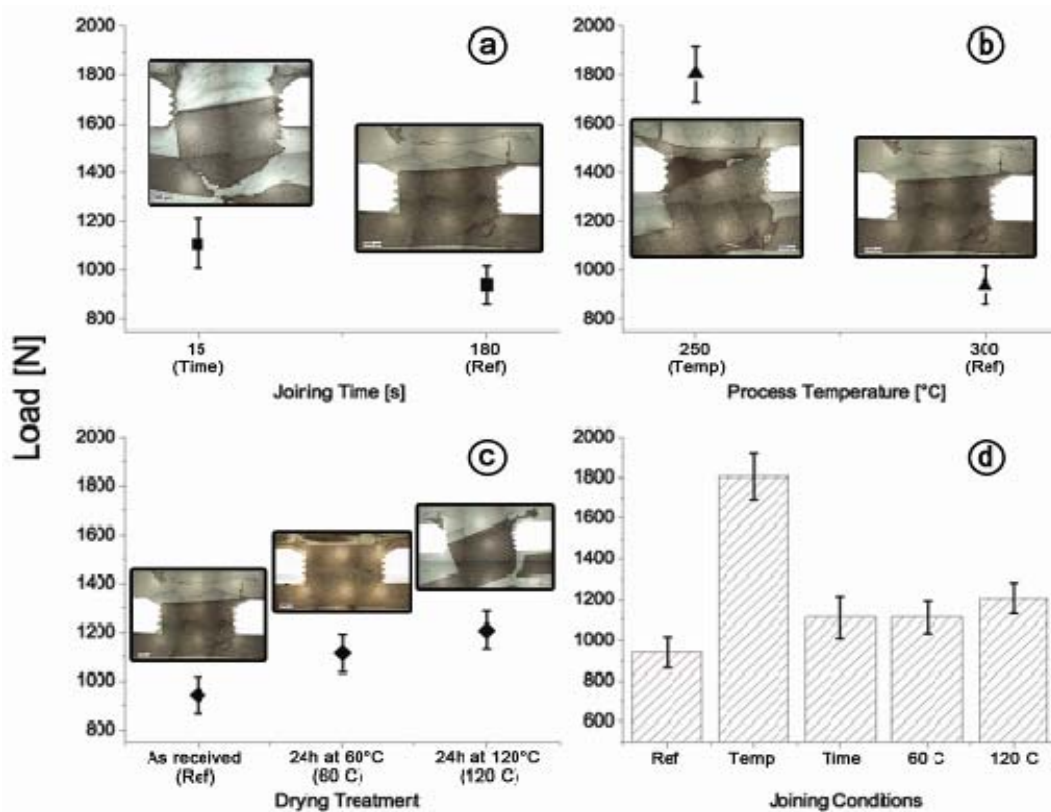
Figure 12: Effects of single parameters on the maximum load of PA66-GF/AA2024 ICJ joints. a) joining time; b) process temperature; c) drying treatment; and d) comparison of the joining conditions.
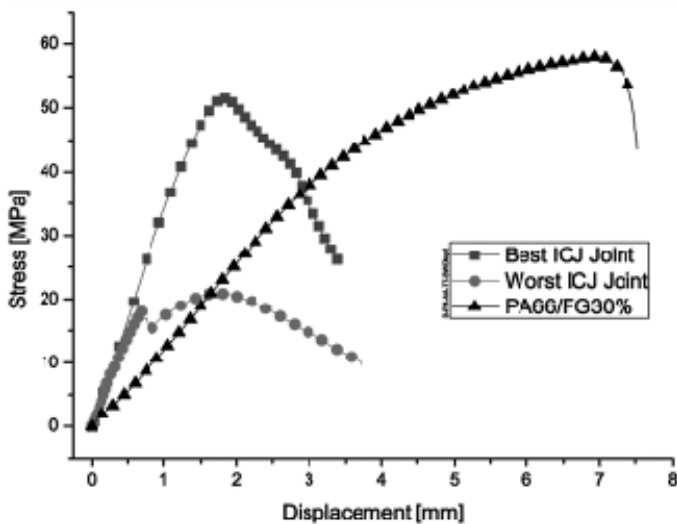

Figure 13: Mechanical performance of the base material PA66-GF (tensile testing) and ICJ hybrid joints between PA66-GF and AA2024 (lap shear testing), exhibiting the best and worst performance observed for this material combination.

TABLES AND TABLE CAPTIONS

Table 1: Joining conditions evaluated in this study.

Parameter	Joining Conditions				
	Ref	**Temp**	**Time**	**60C-PA66**	**120C-PA66**
Processing Temperature	**300 °C**	**250 °C**	300 °C	300 °C	300 °C
Joining Time	**3 min**	3 min	**0,25 min**	3 min	3 min
Drying Treatment	**none**	none	None	**24 h at 60 °C**	**24h at 120 °C**

Table 2: ANOVA results for response "maximum load".

Factor	Levels	Average ± StDev [N]	F	Prob (F)	F-Test
Joining Time	180 s (3 min) 15 s (0,25 min)	942 ± 77 1112 ± 102	7,99	2,55E-02	Significant
Processing Temperature	300 °C 250 °C	942 ± 77 1807 ± 114	186,78	2,64E-06	Significant
Drying Treatment	As received 24h at 60 °C 24h at 120 °C	942 ± 77 1114 ± 79 1208 ± 77	16,71	2,55E-02	Significant